

Use of surfactant in aniline polymerization with TiO_2 to PANI- TiO_2 for supercapacitor performance

Bal Sydulu Singu · Umashankar Male ·
Palaniappan Srinivasan · Srinivas Pabba

Received: 2 December 2013 / Revised: 29 January 2014 / Accepted: 26 February 2014 / Published online: 15 March 2014
© Springer-Verlag Berlin Heidelberg 2014

Abstract Polyaniline sulphate salt titanium dioxide composite (PANI- $\text{H}_2\text{SO}_4\cdot\text{TiO}_2$) was synthesized by chemical in situ polymerization of aniline in the presence of TiO_2 . The effect of anionic surfactant (sodium lauryl sulphate) in this reaction was also assessed. During the polymerization reaction, sodium lauryl sulphate (SLS) is converted to dodecyl hydrogen sulphate (DHS) in the presence of acidic medium and gets doped onto polyaniline along with sulphuric acid dopant, i.e. formation of polyaniline-sulphate-dodecyl hydrogen sulphate-titanium dioxide composite (PANI- $\text{H}_2\text{SO}_4\cdot\text{DHS}\cdot\text{TiO}_2$). In the PANI- $\text{H}_2\text{SO}_4\cdot\text{DHS}\cdot\text{TiO}_2$ composite, the presence of DHS is confirmed by Fourier transform infrared spectroscopy (FTIR), X-ray diffraction (XRD) and energy-dispersive X-ray analysis (EDAX) and TiO_2 is confirmed by XRD and EDAX results. In PANI- $\text{H}_2\text{SO}_4\cdot\text{DHS}\cdot\text{TiO}_2$ system, the nanoparticle of TiO_2 (10–20 nm) is uniformly embedded on nanofibres (20–60 nm) of PANI- $\text{H}_2\text{SO}_4\cdot\text{DHS}$, and some part of PANI- $\text{H}_2\text{SO}_4\cdot\text{DHS}\cdot\text{TiO}_2$ forms core-shell morphology, wherein TiO_2 is in core and PANI- $\text{H}_2\text{SO}_4\cdot\text{DHS}$ in shell forms. Stability of PANI- $\text{H}_2\text{SO}_4\cdot\text{DHS}$ increases due to the incorporation of stable TiO_2 . Utility of PANI- TiO_2 composite was carried out in supercapacitor cell system by performing cyclic voltammetry, galvanostatic charge-discharge and electrochemical impedance spectroscopic techniques in 1 M H_2SO_4 solution. Very low values of solution resistance, charge transfer resistance and time constant are

obtained between 0.2 and 0.6 V. Initial specific capacitance values for the cell carried out at low and high current densities are found to be 280 and 205 F g^{-1} , respectively, and after 1,700 charge-discharge cycles, its retention in the specific capacitance values is found to be the same (65–66 %) with coulombic efficiency of 98–100 %. A capacitor can work even at a high discharge rate. The efficiency of oxidizing and doping power increases with the use of a surfactant. Moreover, the use of a long chain surfactant dopant containing polyaniline as an electrode material plays an important role to increase the performance of the supercapacitor by allowing the electrolyte to easily enter and come out from PANI electrodes.

Introduction

Electrochemical capacitors also called supercapacitors are emerging energy storage devices because of their high power density, long cycle life, short charge-discharge time, ease of handling, weight and size reduction. Such devices can be used either by themselves as a primary power storage source or as an auxiliary power storage source with rechargeable batteries to meet the energy needs for high power applications such as electric vehicles and industrial mobile equipment. There are two types of supercapacitors which differ in the energy storage mechanism involved, namely electrical double-layer capacitor (EDLC) based on ion adsorption and pseudocapacitor (PC) based on electrochemical redox reactions.

The performance of PCs using metal oxides [1–3] and conducting polymers is reported in reviews [4–6]. Among the transition metal oxides, hydrous ruthenium dioxide is recognized as one of the most promising candidates for electrode materials in electrochemical capacitors because of a combination of unique characteristics such as high thermal and chemical stability, low resistivity and remarkable redox

B. S. Singu · S. Pabba
Department of Chemistry, Osmania University, Hyderabad 500 007,
India

U. Male · P. Srinivasan (✉)
Polymers & Functional Materials Division, CSIR-Indian Institute of
Chemical Technology, Hyderabad 500 007, India
e-mail: palani74@rediffmail.com

P. Srinivasan
e-mail: palaniappan@iict.res.in

properties [7]. But the lack of abundance and the cost of the precious metal (Ru) are the major disadvantages for the commercial production of RuO₂. In the recent work, Dunn et al. used a detailed cyclic voltammetric analysis to establish quantitatively the dependence of the pseudocapacitance on the particle size of anatase titanium dioxide (TiO₂) nanocrystals. The results showed that the pseudocapacitive contribution to charge storage increases significantly for particle sizes <10 nm, leading to higher levels of total stored charge and much faster charge/discharge kinetics [8].

Among the conducting polymers, polyaniline (PANI) is a unique and promising candidate for practical applications because of its good processability, environmental stability, low cost and reversible control of electrical properties by simple acid–base doping–dedoping chemistry.

Xiong et al. showed improvement in the electrochemical stability of PANI/TiO₂ in the PANI-TiO₂ composite, which is due to donor–acceptor interactions between PANI and TiO₂ surface [9]. In a review article, Romero had highlighted the improvement of properties of polyaniline-inorganic hybrid materials compared to that of their individual components [10].

Electrochemical properties of PANI-TiO₂ prepared by aqueous [11], in situ [12] and solid state polymerization pathway [13] have been reported in the literature.

The main idea when developing hybrid materials is to take advantage of the best properties of each component that forms the hybrid, trying to decrease or eliminate their drawbacks getting in an ideal way a synergic effect, which results in the development of new materials with new properties.

In this work, PANI-TiO₂ composite was synthesized by aqueous polymerization pathway by oxidizing aniline with ammonium persulphate in the presence of sulphuric acid with and without the use of emulsifier (sodium lauryl sulphate). These composite materials are used as electrode in symmetric supercapacitor cell and their performances were evaluated.

Experimental

Materials and instrumentation

Aniline (S.D. Fine Chemicals, India) was purified under reduced pressure and stored in a refrigerator before use. All other chemicals including ammonium persulphate (APS), sodium lauryl sulphate (SLS), sulphuric acid H₂SO₄ (S.D. Fine Chemicals, India) and TiO₂ (EU consortium, surface area 49 m² g⁻¹) were used as received without further treatment. All the reactions were carried out using distilled water.

The polymer samples for Fourier transform infrared spectroscopy (FTIR) analysis were mixed with KBr powder and compressed into pellets, wherein the sample powder was evenly dispersed in KBr. FTIR spectra were recorded with a

gas chromatography–FTIR spectrometer (model 670, Nicolet Nexus, Minnesota). Powder X-ray diffraction was performed with an X-ray diffractometer (Karlsruhe, Germany) with Cu K_α radiation ($\lambda=1.54 \text{ \AA}$). Powder samples were used by employing a standard sample holder. The d-spacing was calculated from the angular position 2θ of the observed reflection peaks based on the Braggs formula ($2d\sin\theta=n\lambda$), where λ is the wavelength of the X-ray beam and θ is the diffraction angle. Morphology studies of the polymer powder samples were carried out with Hitachi S-4300 SE/N field emission scanning electron microscope (FESEM) (Hitachi, Tokyo, Japan) operating at 20 kV. The PANI-TiO₂ powder sample was sputtered on a carbon disc with the help of double-sided adhesive tape. Thermogravimetric analysis (TGA) was performed with a TA Instruments TGA Q500 Universal at a heating rate of 10 °C min⁻¹ under nitrogen atmosphere. Transmission electron microscopy (TEM) measurement was performed by casting sample dispersion on carbon-coated copper grids and allowing it to dry at room temperature. Measurements were done on TECNAI G2 F30 S-TWIN instrument operated at an accelerate voltage of 200 kV with a lattice resolution of 0.14 nm and point image resolution of 0.20 nm.

Electrochemical testing

The polymer sample electrode was fabricated by pressing the sample on stainless steel mesh by the application of 120 kg cm⁻² of pressure. The electrochemical performances of all the polymer samples were investigated using two-electrode system cells without a reference electrode. Two electrodes with identical sample were assembled as supercapacitor, the electrolytic solution used was 1 M H₂SO₄ and cotton cloth was utilized as a separator. Cyclic voltammetry and galvanostatic charge–discharge experiments were carried out with a WonATech multichannel potentiostat/galvanostat (WMPG1000, Gyeonggi-do, South Korea). Cyclic voltammograms (CV) were recorded from –0.2 to 0.8 V at various sweep rates, and charge–discharge experiments were carried out from 0 to 0.6 V at various current densities. Electrochemical impedance spectroscopy (EIS) measurements were carried out with IM6ex (Zahner-Elektrik, Germany) by applying an AC voltage of 5 mV amplitude in the 40-kHz to 10-mHz frequency range at various voltages using three-electrode cell configuration, i.e. polymer electrode as working electrode, platinum counter electrode and calomel electrode as reference electrode. All electrochemical measurements were carried out at room temperature.

Synthesis of PANI-DHS-H₂SO₄ (SPANI)

In a typical synthesis, 0.25 ml of aniline and sodium lauryl sulphate surfactant (38 mg) were dissolved in 50 ml of 1 M

H_2SO_4 taken in 250-ml round-bottomed flask, and 0.61 g of ammonium persulphate was dissolved in 50 ml of 1 M H_2SO_4 in a 100-ml beaker. Both the solutions were mixed together and the resulting reaction mixture was stirred for 24 h at ambient temperature. The reaction mixture was poured into 250 ml of acetone. The precipitate was filtered and washed with an ample amount of water and acetone. The sample was dried at 50 °C till a constant weight.

Synthesis of PANI- $\text{H}_2\text{SO}_4 \cdot \text{TiO}_2$ composite

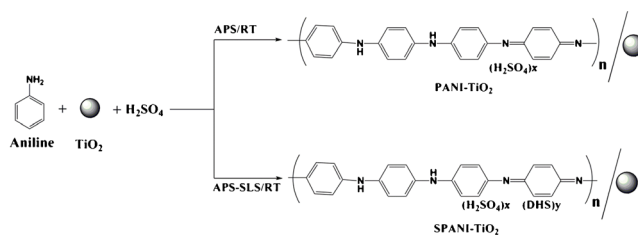
Polyaniline-titanium dioxide composite was synthesized by following the reported procedure [11]. In a typical synthesis, 0.25 ml of aniline was dissolved in 50 ml of 1 M H_2SO_4 taken in 250-ml round-bottomed flask, then a particular amount of TiO_2 was added and the mixture was stirred for about 30 min. of ammonium persulphate, 0.61 g was dissolved in 50 ml of 1 M H_2SO_4 . Both the solutions were mixed together and the resulting reaction mixture was stirred for 24 h at ambient temperature. The reaction mixture was poured into 250 ml acetone. The precipitate was filtered and washed with an ample amount of water and acetone. The sample was dried at 50 °C till a constant weight.

Synthesis of PANI-DHS- $\text{H}_2\text{SO}_4 \cdot \text{TiO}_2$

Synthesis of polyaniline salt was carried out by the above procedure using anionic surfactant, i.e. sodium lauryl sulphate surfactant (38 mg) was added along with 0.25 ml of aniline in 50 ml of 1 M H_2SO_4 solution.

Results and discussion

Polyaniline- TiO_2 composite powders were prepared by aqueous polymerization pathway by oxidizing aniline in the presence of various amounts of TiO_2 using sulphuric acid as protonic acid and ammonium persulphate as oxidant. The effect of SLS surfactant in the reaction was also studied (Scheme 1). The composites synthesized without SLS are labelled as PANI- TiO_2 -XX with the use of SLS as SPANI- TiO_2 -XX, where XX represents the amount of TiO_2 used in the reaction. Polymerization reaction yields and the value of specific capacitances calculated from cyclic voltammetry of PANI- TiO_2 and SPANI- TiO_2 composites with various scan rates are reported in Table 1. The value of yield of the composites increases with increasing the amount of TiO_2 in the reaction mixture. An increase in yield is due to an increase in the amount of TiO_2 used in the reaction and also TiO_2 acts as template for the nucleation of aniline. The value of yield is further increased with the use of SLS due to increasing the efficiency of oxidation of aniline monomer by SLS, wherein SLS is converted to dodecyl hydrogen sulphate (DHS) and



Scheme 1 Schematic representation of the synthesis of PANI- TiO_2 and SPANI- TiO_2 composites

gets incorporated on polyaniline as dopant. Specific capacitance value increases up to 30 wt% of TiO_2 and then decreases. An increase in capacitance with TiO_2 is due to the nucleation of aniline by TiO_2 , and after 30 wt%, capacitance value decreases due to the involvement of more amount of semiconducting TiO_2 , which decreases the conductivity of polyaniline salt. The increase in specific capacitance of SPANI- TiO_2 composites relative to PANI- TiO_2 is due to the presence of long chain alkyl group on polyaniline salt as dopant, which allows the electrolyte to penetrate into polyaniline salt electrode. Further, among SPANI- TiO_2 samples, SPANI- TiO_2 -30 shows higher specific capacitance as seen from cyclic voltammetry results, so further characterization is carried and discussed for the SPANI- TiO_2 -30 sample.

The electrochemical capacitance performance of all the PANI- TiO_2 composites was tested by carrying out the CV of symmetrical cell system. Cell was assembled with two identical electrodes of PANI- TiO_2 material with a cotton cloth separator containing 1 M aq. H_2SO_4 electrolyte. CV was recorded from -0.2 to 0.8 V at various sweep rates, and the specific capacitance (C_s) values are reported in Table 1. Generally, the value of C_s for the sample prepared with the use of SLS in the reaction is found to be higher than that of the sample prepared without SLS. As a representative system, the value of C_s for SPANI- TiO_2 -30 carried out at 1 mV s^{-1} scan rate is higher (359 F g^{-1}) compared to that of PANI- TiO_2 -30 (230 F g^{-1}), which in turn higher than that of PANI- H_2SO_4 (195 F g^{-1}) [14]. Among the SPANI- TiO_2 samples, SPANI- TiO_2 -30 shows higher capacitance value. Hence, CV of the cell with the use of SPANI- TiO_2 -30 material at various scan rates (1, 5, 10, 20, 50, 100 and 200 mV s^{-1}) are carried out (Fig. 1), and the corresponding specific capacitances are found to be 359, 356, 300, 221, 138, 100 and 84 F g^{-1} , respectively. At slower scan rates, the diffusion of ions from the electrolyte can gain access to almost all available materials of the electrode, leading to an effective insertion and de-insertion processes. But, when the scan rate is increased, the effective interaction between the ions and the electrode is greatly reduced, and redox reaction has been limited only to the outer surface of electrode; hence, there is a reduction in capacitance [15, 16]. Another observation is that even with very high scan rate at 200 mV s^{-1} , the shape of the CV curve was still maintained and this demonstrates high performance of the

Table 1 Yield and specific capacitance values at different scan rates of PANI composites prepared with and without SLS by aqueous polymerization pathway

System	TiO ₂ weight (mg)	Yield (mg)	Specific capacitance (F g ⁻¹)								
			1	2	5	10	20	30	40	50	100
a											
SPANI-TiO ₂ -10	10	130	168	184	159	137	117	98	81	70	41
SPANI-TiO ₂ -20	20	170	186	–	145	124	101	98	79	70	50
SPANI-TiO ₂ -30	30	180	359	358	356	300	221	192	175	138	100
SPANI-TiO ₂ -40	40	190	209	179	165	151	141	135	127	119	92
SPANI-TiO ₂ -50	50	200	175	168	152	122	120	108	94	85	57
b											
PANI-TiO ₂ -10	10	100	129	104	101	99	94	88	86	83	72
PANI-TiO ₂ -20	20	140	162	122	111	104	111	104	91	83	79
PANI-TiO ₂ -30	30	160	230	210	180	170	158	142	120	95	89
PANI-TiO ₂ -40	40	180	179	115	102	87	98	96	92	90	84
PANI-TiO ₂ -50	50	190	139	128	119	112	109	101	93	89	78

a reaction conditions: aniline (0.25 ml), SLS (38 mg), APS (0.61 g), time (24 h) and various amounts of TiO₂ in milligrams; *b* reaction conditions: aniline (0.25 ml), APS (0.61 g), time (24 h) and various amounts of TiO₂ in milligrams

supercapacitor (Fig. 1) [17]. The superior rate capability of SPANI-TiO₂-30 composite electrodes can be attributed to the high activated surface and increased electrical conductivity due to the synergistic contribution of polyaniline-coated TiO₂. Among the polyaniline salts, SPANI-TiO₂-30 shows better performance and, hence, spectral, thermal and electrochemical performances are carried out for SPANI-TiO₂-30 and the results are discussed here.

Fourier transform infrared spectra of SPANI, TiO₂ and SPANI-TiO₂-30 samples are shown in Fig. 2. TiO₂ shows peaks at 3,400 and 1,650 cm⁻¹ (Fig. 2c) due to surface-adsorbed water and hydroxyl groups, respectively [18]. The sharp band present below 850 cm⁻¹ is due to the lattice vibrations of TiO₂ [19]. The IR spectrum of SPANI (Fig. 2a) shows major characteristic peaks of polyaniline salt at around

3,425 cm⁻¹ (N–H stretching), 3,220 cm⁻¹ (NH⁺—indicative of doping, i.e. salt formation), 1,560–1,565 cm⁻¹ (C=C stretching, quinonoid ring), 1,465–1,490 cm⁻¹ (C=C stretching, benzenoid ring), 1,300 cm⁻¹ (C–N stretching, quinonoid ring), 1,225–1,240 cm⁻¹ (C–N stretching, benzenoid ring), 1,120–1,140 cm⁻¹ (N=Q=N vibration, where Q represents the quinonoid ring) and 800 cm⁻¹ (1,4-disubstituted benzene). Infrared spectrum of SPANI-TiO₂-30 (Fig. 2b) shows peaks due to normal polyaniline and, in addition, it shows a peak at 1,730 cm⁻¹ which indicates overoxidation and peaks at 1,640 and 1,030 cm⁻¹ due to SO₃H group, which confirms the presence of DHS as a dopant on polyaniline.

X-ray diffractograms of SPANI, TiO₂ and SPANI-TiO₂-30 are shown in Fig. 3. X-ray diffraction (XRD) spectrum of TiO₂ shows peaks at d-spacing of 3.51, 2.42, 2.37, 2.33, 1.89, 1.69, 1.66 and 1.48 Å (Fig. 3a), which corresponds to the anatase form of TiO₂ (authenticated with the standard Joint

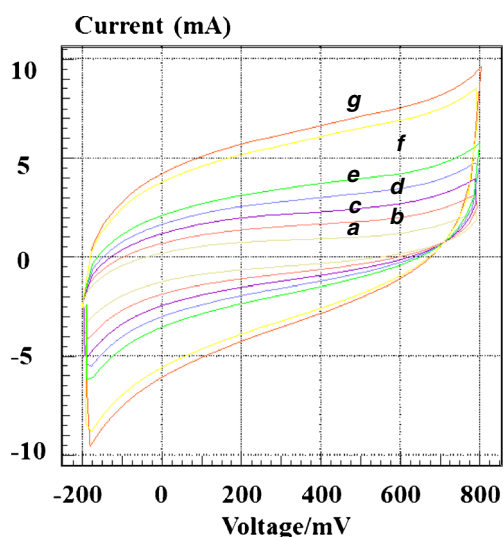


Fig. 1 Cyclic voltammograms of symmetric cell of SPANI-TiO₂-30 in 1 M H₂SO₄ electrolyte at various sweep rates (*a*) 1, (*b*) 5, (*c*) 10, (*d*) 20, (*e*) 50, (*f*) 100 and (*g*) 200 mV s⁻¹

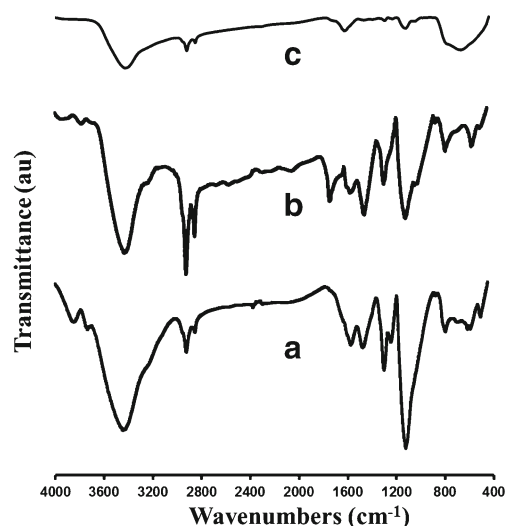


Fig. 2 FTIR spectra of (*a*) SPANI, (*b*) SPANI-TiO₂-30 and (*c*) TiO₂

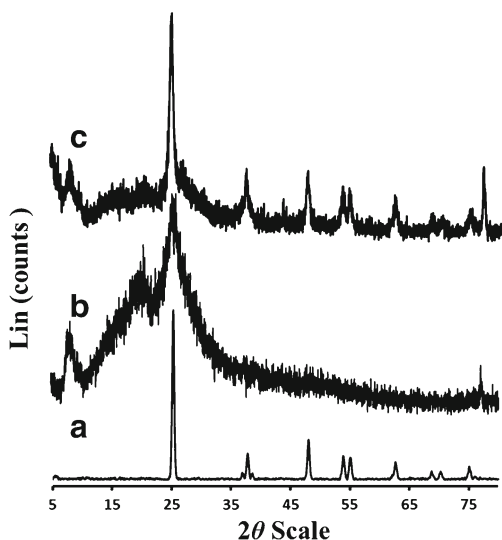
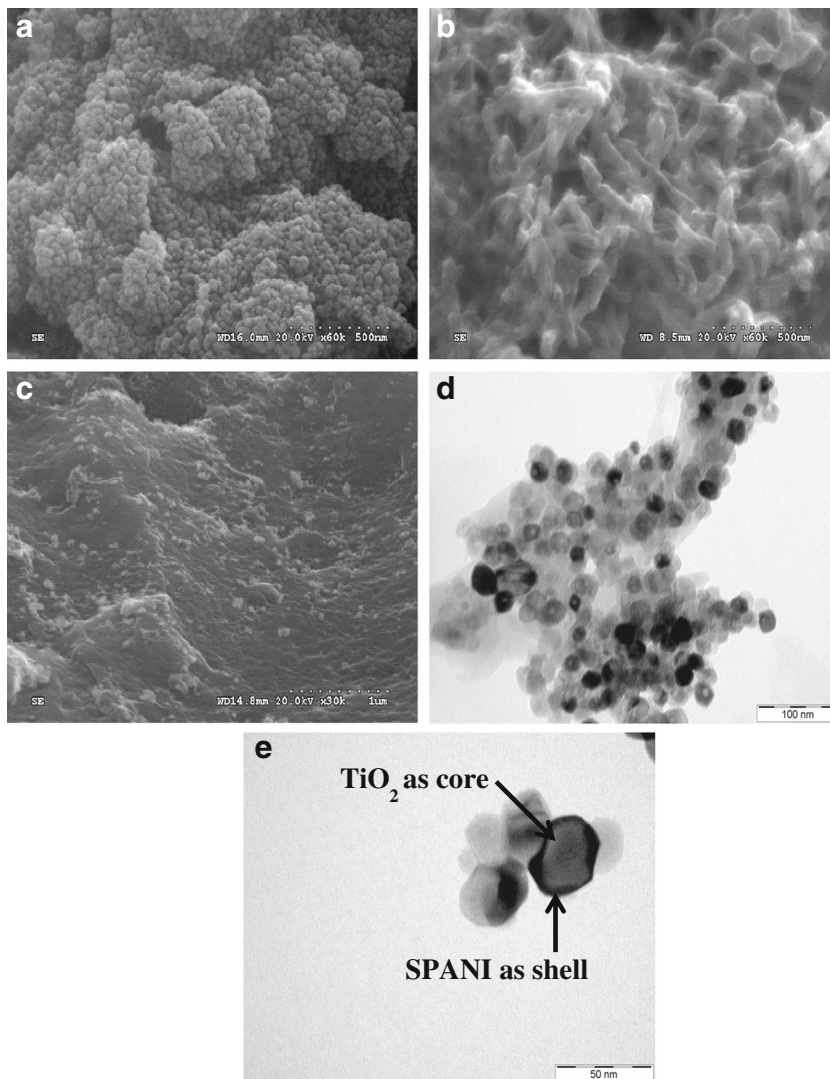


Fig. 3 XRD patterns of (a) TiO₂, (b) SPANI and (c) SPANI-TiO₂-30

Committee on Powder Diffraction Standards (JCPDS) values; JCPDS No. 21-1272). The XRD spectrum of SPANI shows three broad peaks corresponding to d-spacings at 10.85, 7.71 and 4.26 Å (Fig. 3b). The peaks at d-spacings of 7.71 and 4.26 Å correspond to PANI salt, and a peak at 10.85 Å is due to long chain dopant in polyaniline salt. In this case, the long chain is DHS which is obtained during the oxidation of aniline in the presence of dilute sulphuric acid and sodium lauryl sulphate by ammonium persulphate, wherein sodium lauryl sulphate is converted to dodecyl hydrogen sulphate in the presence of acid and gets doped onto polyaniline. This result indicates that SPANI contains DHS as the dopant. XRD of SPANI-TiO₂-30 shows peaks corresponding to d-spacings at 10.85, 7.71, 4.26, 3.53, 2.37, 1.89, 1.70, 1.67, 1.48, 1.36, 1.33 and 1.26 Å (Fig. 3c). In the SPANI-TiO₂-30 composite, the first three peaks indicate the presence of SPANI, and the remaining peaks indicate the presence of TiO₂. Broad peaks are observed for TiO₂ in the SPANI-TiO₂-30 composite

Fig. 4 FESEM images of (a) TiO₂, (b) SPANI and (c) SPANI-TiO₂-30 and (d, e) TEM image of SPANI-TiO₂-30



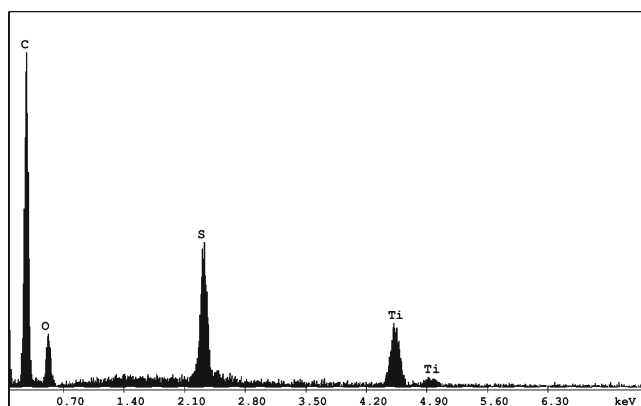


Fig. 5 EDAX spectrum of SPANI-TiO₂-30

compared to pure TiO₂ indicating the decrease in crystallinity of TiO₂.

Morphologies of SPANI, TiO₂ and its composite SPANI-TiO₂-30 were determined by FESEM and are shown in Fig. 4. The FESEM of TiO₂ shows agglomerated nanospheres with a diameter of 10–20 nm (Fig. 4a), SPANI shows nanofibre form with a diameter of 20–60 nm (Fig. 4b) and, in SPANI-TiO₂-30 composite, particles of TiO₂ are uniformly spread on the polyaniline (Fig. 4c). In order to find out the better morphological information, TEM analysis was carried out for SPANI-TiO₂-30. TEM image at low resolution shows that nanospheres of TiO₂ (10–15 nm) are embedded uniformly in PANI matrix (Fig. 4d), and the high-resolution TEM shows that some of the nanospheres of TiO₂ are uniformly coated by PANI, wherein TiO₂ (dark particles) present as core material and the amorphous PANI present as shell (Fig. 4e) and remaining TiO₂ particles are embedded in PANI matrix.

EDAX spectrum of SPANI-TiO₂-30 is shown in Fig. 5, and it shows the presence of Ti and S elements. The presence of

Table 2 Specific capacitance, energy density and power density at various charge–discharge specific current densities for SPANI-TiO₂-30 cell system

Specific current density (A g ⁻¹)	C _d (F g ⁻¹)	Energy density (Wh kg ⁻¹)	Power density (W kg ⁻¹)
0.2	355	17.7	200
0.4	280	12.6	230
2.0	205	10.3	1,020
4.0	200	10.1	1,750

elements S indicates the presence of SO₃H group, which might have come from sulphuric acid/SLS surfactant, and the element Ti shows the presence of titanium oxide.

Thermal stability of SPANI-TiO₂-30 is compared with that of its individual components, SPANI and TiO₂, by carrying out thermogravimetric analysis (TGA) under nitrogen atmosphere (Fig. 6). TGA thermogram shows that TiO₂ is highly stable and it shows only 5 wt% loss up to 700 °C. However, SPANI and SPANI-TiO₂-30 show weight loss up to 110 °C due to moisture present on the polymer chain, and they are stable up to around 210 °C. Weight loss observed for SPANI and SPANI-TiO₂-30 at degradation point is 15 and 13 %, respectively. Higher stability of SPANI-TiO₂-30 compared to that of SPANI is due to the presence of stable TiO₂ in the composite [20, 21].

For practical applications, supercapacitor must have long-term cycle stability. The stability of the supercapacitor cell for symmetric SPANI-TiO₂-30 electrode in 1 M aqueous H₂SO₄ electrolyte was evaluated by galvanostatic charge–discharge measurement at low (0.4 A g⁻¹) and high current densities (2.0 A g⁻¹) in the potential range between 0 and 0.6 V for

Fig. 6 Thermograms of (a) TiO₂, (b) SPANI-TiO₂-30 and (c) SPANI

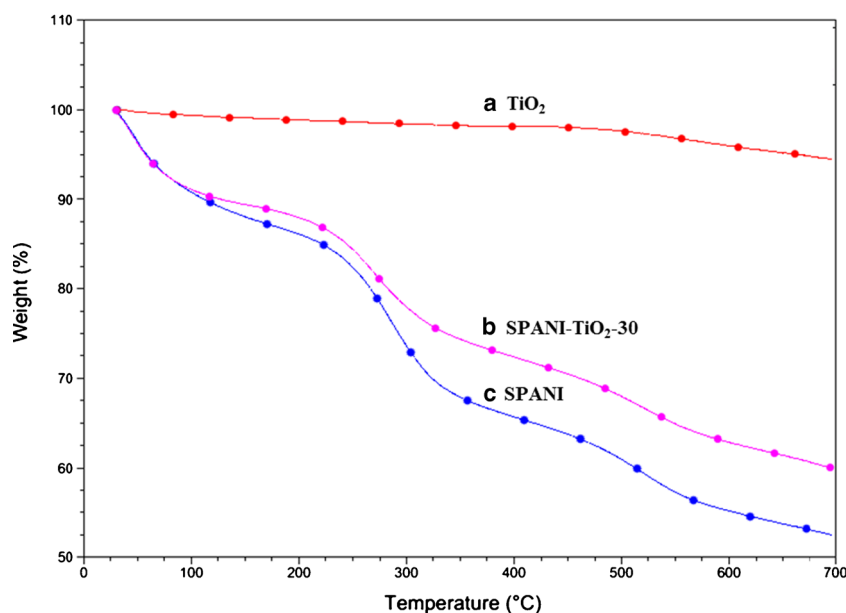
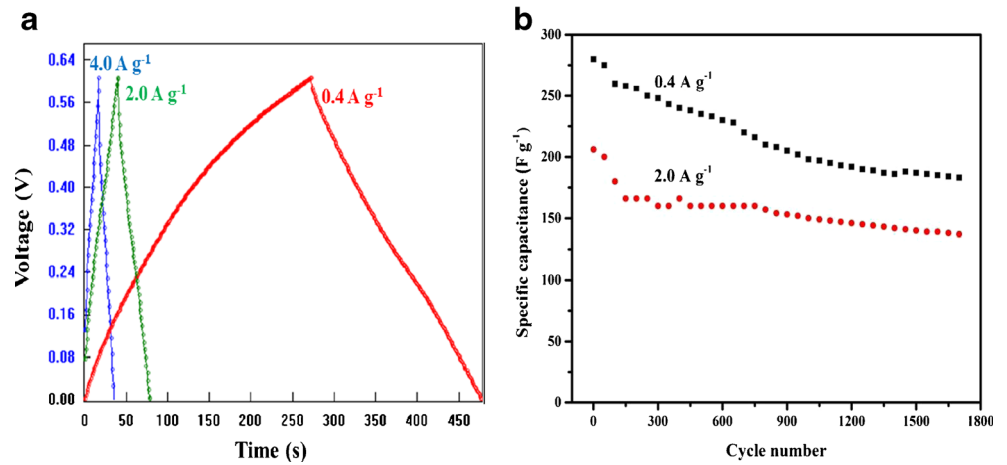


Fig. 7 SPANI-TiO₂-30 cell in 1 M H₂SO₄ electrolyte. (a) Galvanostatic charge–discharge curves at 0.4, 2.0 and 4.0 A g⁻¹ current densities and (b) cycle life at 0.4 and 2.0 A g⁻¹ current densities



1,700 cycles. The potential versus time plot in the charge/discharge experiment for an ideal capacitor should be ‘Λ’-

shaped curve. In the case of EDLC, generally, the charge/discharge curves are obtained almost Λ-shaped curve (no

Fig. 8 EIS of SPANI-TiO₂-30: Nyquist plot with the inset of circuit diagram carried out at (a) 0.2 V, (b) 0.4 V and (c) 0.6 V and corresponding plot of (d) frequency versus specific capacitance and (e) frequency versus phase angle

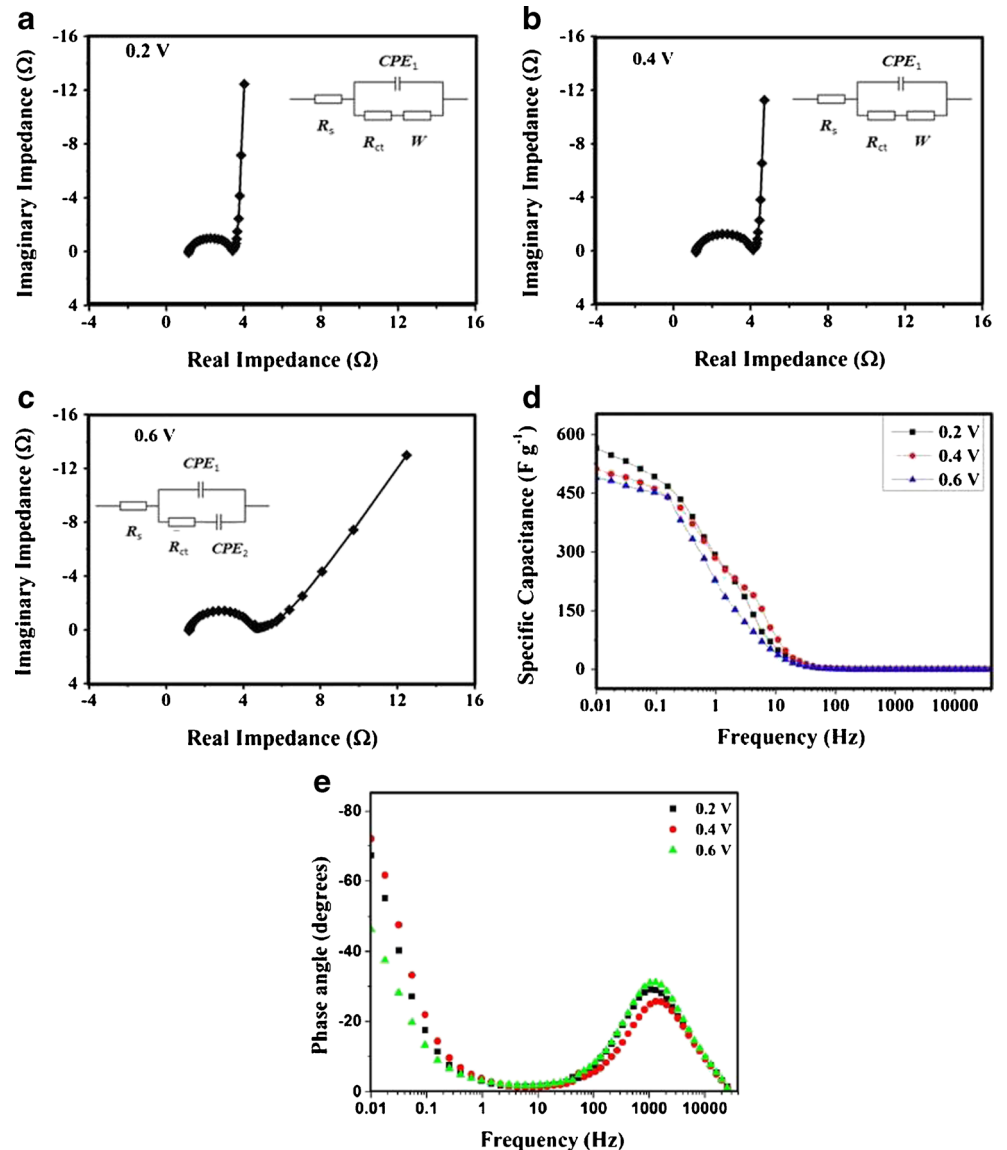


Table 3 Solution resistance (R_s), charge transfer resistance (R_{ct}), time constant (τ) and specific capacitance (C_s) for SPANI-TiO₂-30 sample

Voltage (V)	R_s (Ω)	R_{ct} (Ω)	τ (ms)	C_s at 10 mHz ($F\ g^{-1}$)
0.2	1.16	2.94	0.18	510
0.4	1.15	2.28	0.19	565
0.6	1.18	3.56	0.30	490
0.8	1.41	86.09	3.78	260

significant faradaic process occurs) which indicates the material has good charge–discharge reversibility [22]. Whereas in the case of pseudocapacitor, distorted λ -shaped curve is observed because of redox reaction during charge and discharge process (faradaic process). Also, a small initial voltage drop is observed in the charge/discharge experiment due to bulk solution resistance, electrode resistance and ion migration resistance in the electrode [23]. The values of discharge-specific capacitance, energy and power densities are calculated at various discharge current densities, and the values are reported in Table 2. The values of C_d , ED and PD calculated at 0.2 A g^{-1} current density are 355 $F\ g^{-1}$, 17.7 $Wh\ kg^{-1}$ and 200 $W\ kg^{-1}$, respectively. Cell was subjected to 1,700 charge–discharge cycles at low (0.4 A g^{-1}) and high (2 A g^{-1}) current densities. Initial C_s values carried out at low and high current densities are found to be 280 and 205 $F\ g^{-1}$, respectively, and after 1,700 charge–discharge cycles, its retention in the specific capacitance values is found to be 65 and 66 % (Fig. 7), respectively, with coulombic efficiency of 98–100 %. Better performance of supercapacitor even at high discharge rate is due the presence of long chain surfactant molecule as the dopant on polyaniline electrode material allows the electrolyte to easily enter and come out from PANI electrodes.

EIS is an important analytical technique used to gain information about the characteristic frequency responses of supercapacitors and the capacitive phenomena occurring in the electrodes. EIS experiment was carried out for SPANI-TiO₂-30 sample in the frequency range from 40 kHz to 10 mHz at applied voltages of 0.2, 0.4, 0.6 and 0.8 V (Fig. 8), and the EIS parameters are reported in Table 3. The value of solution resistance (R_s) is found to be almost the same (around 1.15 Ω) with voltages of 0.2, 0.4 and 0.6 V indicating the good conductivity of the electrolyte and the very low

internal resistance of the electrode. However, the value of solution resistance increased at 0.8 V (1.41 Ω). The values of time constant (τ) increase with increasing the voltage, i.e. 0.18, 0.19, 0.30 and 3.78 ms at 0.2, 0.4, 0.6 and 0.8 V, respectively. Lower time constants observed between 0.2 and 0.6 V indicates the fast charge–discharge process [24, 25]. The value of charge transfer resistance (R_{ct}) is the main part of resistance of the supercapacitor. If the materials show less in the charge transfer resistance, it has high in electrical conductivity and fast response ability of the electrode. The value of charge transfer resistance is found to be almost the same (around 3 Ω) with voltages of 0.2, 0.4 and 0.6 V indicates high in electrical conductivity and fast response ability of the electrode. However, the value of charge transfer resistance at 0.8 V (86 Ω) indicates the polyaniline in its de-doped state [26]. A very low value of R_s , R_{ct} and τ obtained between 0.2 and 0.6 V indicates fast charge–discharge process, low ESR and high electrical conductivity of the electrode/electrolyte. The results of R_s , R_{ct} , τ and C_s show that the use of the supercapacitor cell at 0.8 V may not be good.

The specific capacitance of SPANI-TiO₂-30 calculated at 0.2, 0.4, 0.6 and 0.8 V was 510, 565, 490 and 260 $F\ g^{-1}$, respectively, at 10 mHz frequency. The operating frequency (the frequency at which the capacitance is 50 % of its maximum value) of SPANI-TiO₂-30 carried out at 0.2, 0.4 and 0.6 V is 0.8, 2.1 and 35 Hz, respectively (Fig. 8d), corresponding to the characteristic relaxation times 1.2, 0.5 and 0.03 s, respectively [27].

Capacitor response frequencies for the system of SPANI-TiO₂-30 at three applied voltages, i.e. 0.2, 0.4 and 0.6 V, was calculated from the bode plot of frequency versus phase angle (Fig. 8e). The upper limit of the low-frequency region is defined as the capacitor response frequency $f_{\phi=-45^\circ}$, which is the frequency interpolated at $\phi=-45^\circ$ in the frequency versus phase angle graph. The capacitor response frequencies at 0.2, 0.4 and 0.6 V are 0.04, 0.04 and 0.09 Hz, respectively, and the corresponding response times are 25, 25 and 11 s, respectively [28].

The equivalent circuit model was obtained using commercial built-in software packages of the electrochemical workstations. Equivalent circuit diagrams of SPANI-TiO₂-30 at 0.2, 0.4 and 0.6 V are shown in the inset of Fig. 8. In the case of 0.2 and 0.4 V, R_{ct} and W arranged in serial manner and parallel to the constant phase element (CPE)₁ (double-layer capacitive element) and series to the R_s . When increasing the applied potential to 0.6 V, the same equivalent circuit diagram

Table 4 Equivalent circuit diagram parameters for SPANI-TiO₂-30 sample

Voltage (V)	R_s (Ω)	R_{ct} (Ω)	W/Ω	n	CPE ₁ (mF)	n	CPE ₂ (mF)	n
0.2	1.17	2.80	1.12	0.98	0.21	0.95	–	–
0.4	1.16	2.27	1.15	0.96	0.19	0.93	–	–
0.6	1.19	3.18	–	–	0.16	0.91	332	0.52

is reproduced, but in the place of W , CPE_2 is present (pseudocapacitive element).

EIS parameters for SPANI-TiO₂-30 are reported in Table 4. The frequency power obtained by fitting of suitable circuit showed that SPANI-TiO₂-30 exhibited towards more ideal capacitive behaviour at 0.2 V ($n=0.95$) than at 0.4 V ($n=0.93$) and at 0.6 V ($n=0.91$). The value of solution resistance and charge transfer resistance carried out at 0.2, 0.4 and 0.6 V calculated from the circuit diagram are found to be very near the same with that of the value calculated from the semicircle high-frequency region.

Conclusions

Long chain surfactant molecule is successfully introduced as a dopant to polyaniline-sulphate salt along with titanium dioxide to PANI-H₂SO₄-DHS·TiO₂, a core-shell nanocomposite, wherein TiO₂ is in core and PANI-H₂SO₄-DHS in shell form. Core-shell PANI-TiO₂ composite containing DHS and H₂SO₄ dopants is used as a high-performance electrode material in supercapacitor via the incorporation of long chain surfactant molecule (DHS) onto polyaniline which allows the electrolyte to easily enter and come out from PANI electrodes.

Acknowledgments We thank the Department of Science and Technology, New Delhi for funding under the project DST/TSG/PT/2011/179-G. We also thank Dr. Vijayamohan K. Pillai, Director, CSIR-CECRI, Karaikudi for his valuable discussion. SBS and PS are thankful to IICT for carrying out this work at IICT, SBS is thankful to UGC for providing research fellowship and MU is thankful to CSIR, India for financial assistance.

References

1. Chae JH, Ng KC, Chen GZ (2010) Proc Inst Mech Eng PART A- J Power Energy 220:479–503

2. Weifeng W, Xinwei C, Weixing C, Douglas GI (2011) Chem Soc Rev 40:1697–1721
3. Simon P, Gogotsi Y (2008) Nat Mater 7:845–854
4. Snook GA, Kao P, Best AS (2011) J Power Sources 196:1–12
5. Chang L, Feng L, Lai-Peng M, Hui-Ming C (2010) Adv Mater 22: E28–E62
6. Lijia P, Hao Q, Chunmeng D, Yun L, Lin P, Jianbin X, Yi S (2010) Int J Mol Sci 11:2636–2657
7. Ryu KS, Jeong SK, Joo J, Kim K (2007) J Phys Chem B 111:731–743
8. Wang J, Polleux J, Lim J, Dunn B (2007) J Phys Chem C 111:14925–14931
9. Xiong S, Phua SL, Dunn BS, Ma J, Lu X (2010) Chem Mater 22: 255–260
10. Romero PG (2001) Adv Mater 13:163–174
11. Chaoqing B, Aishui Y, Haoqing W (2009) Electrochem Comm 11: 266–269
12. Xingwei L, Han Z, Gengchao W, Zhihui J (2010) J Mater Chem 20: 10598–10601
13. Tursun A, Aminam U, Ruxangul J, Yuchuan T, Tunsagul A, Ismayil N (2012) J Appl Polymer Sci 126:697–705
14. Sydulu SB, Palaniappan S, Srinivas P (2013) Electrochim Acta 95: 251–259
15. Malak A, Fic K, Lota G, Vix-Guterl C, Frackowiak E (2010) J Solid State Electrochem 14:811–816
16. Subramanian V, Zhu H, Vajtai R, Ajayan PM, Wei B (2005) J Phys Chem B 109:20207–20214
17. Qian C, Jie T, Jun M, Han Z, Norio S, Lu-Chang Q (2011) Carbon 49: 2917–2925
18. Ding Z, Lu GQ, Greenfield PF (2000) J Phys Chem B 104:4815–4820
19. Nakamura R, Imanishi A, Murakoshi K, Nakato Y (2003) J Am Chem Soc 125:7443–7450
20. Zhang X, Ji LY, Zhang SC, Yang WS (2007) J Power Sources 173: 1017–1023
21. Sheng L, Xiaohong L, Zhangpeng L, Shengrong Y, Jinqing W (2011) New J Chem 35:369–374
22. Qu DY (2002) J Power Sources 109:403–411
23. Guo QH, Zhou XP, Li XY, Chen SL, Seema A, Greiner A, Hou HQ (2009) J Mater Chem 19:2810–2816
24. Girija TC, Sangaranarayanan MV (2006) J Power Sources 156:705–711
25. Burke A (2000) J Power Sources 91:37–50
26. Sutar D, Menon R, Subramanyam SV (2002) Thin Solid Films 417: 40–42
27. Xiaowei Y, Junwu Z, Ling Q, Dan L (2011) Adv Mater 23:2833–2838
28. Diah S, Dah-Shyang T, Ying-Sheng H, Alexandru K, Wen-Hung C (2007) J Phys Chem C 111:9530–9537